Study on the Asymptotic Behavior of the Interplay of Stimulated Brillouin Scattering and Brillouin-Enhanced Four-Wave Mixing in Standard Single-Mode Fibers

Kyoungyoon Park

Department of Electrical and Computer Engineering at Seoul National University, Seoul 06288, Korea

Currently with Semiconductor R&D center, Samsung Electronics, Hwaseong-si, Gyeonggi-do 18448, Korea

Achar V. Harish

Optoelectronics Research Centre, University of Southampton, SO17 1BJ, UK

Currently with the Department of Physics, Karnataka University Dharwad, Dharwad 580008, India

Johan Nilsson

Optoelectronics Research Centre, University of Southampton, SO17 1BJ, UK

Yoonchan Jeong

Department of Electrical and Computer Engineering at Seoul National University, Seoul 06288, Korea

Also with ISRC and IAP at Seoul National University, Seoul 06288, Korea

We theoretically study stimulated Brillouin scattering (SBS) in a standard single-mode fiber (SMF), taking Brillouin-enhanced four-wave-mixing (BEFWM) effects into account. In particular, we investigate the case when there is non-negligible back-reflection of the forward-pump field at the rear fiber end although such reflection is typically weak and undesired. We first justify that BEFWM can be treated as a steady-state process under an undepleted pump approximation as long as the nominal SBS gain remains as low as 40 dB unless the pump, Stokes, anti-Stokes fields interact under near perfect phase-matching condition, which hardly happens in normal circumstances with a standard SMF. Under the steady-state and undepleted-pump condition, we find analytical solutions to the Stokes and anti-Stokes fields generated by the forward and backward-pump fields, and also derive their asymptotic formulae in both infinitesimal and infinite limits in terms of the phase-mismatch parameter of $|\Delta kL|$, assuming that both seeding Stokes and anti-Stokes fields arise from white background noise components. When $|\Delta kL| \ll 1$, the acoustic fields driven by SBS and BEFWM tend to interfere destructively, and thus, SBS and BEFWM are anti-resonant to each other, thereby eventually resulting in both Stokes and anti-Stokes scatterings minimized at $\Delta k = 0$. When $|\Delta kL| \gg 1$, all the asymptotic curves for the amplification ratios and extra gain factor obey the inverse square law with respect to $|\Delta kL|$, irrespective of the level of the back-reflection at the rear fiber. In particular, when $|\Delta kL|$ is in the intermediate range where the FWM gain remains relatively large, SBS and BEFWM can be cooperative via the phase-pulling effect by the FWM gain, thereby leading to quasi-resonant growths of both Stokes and anti-Stokes fields. However, the extra gain by BEFWM reduces significantly if the level of the back-reflection remains below one percent, irrespective of the value of $|\Delta kL|$. Since the interplay between SBS and BEFWM is inherently phase-dependent whilst it can still happen with white noise seeding with random phases, the related mechanism can further be exploited for all-optical switching functionality. We expect our theoretical modeling and formulation will be be useful for designing and analyzing a

variety of fiber systems that incorporate high-power narrow-linewidth light undergoing non-negligible back-reflection under various conditions.

Keywords: Fiber lasers, stimulated Brillouin scattering, Brillouin-enhanced four-wave mixing.

Email: yoonchan@snu.ac.kr

I. INTRODUCTION

Stimulated Brillouin scattering (SBS) involves nonlinear scattering of an incident optical field with narrow-linewidth by acoustic fields. The incident optical field pumps a Brillouin-active medium through electrostriction, which normally generates and amplifies a counter-propagating (i.e., backward-propagating) Stokes field down-shifted relative to the incident "pump" field's frequency [1, 2]. Whilst SBS can be utilized as an amplifying mechanism for Brillouin lasers, it can also degrade the performance of fiber laser sources, severely limiting their power-scaling [3-6]. It is especially detrimental for pump linewidths narrower than the Brillouin gain bandwidth of a few tens of MHz, including so-called single-frequency light. Therefore, accurate prediction of the power-limit by SBS is of great importance when designing and operating such a system, and thus has been receiving a considerable amount of attention [1-6].

A complication of the SBS analysis is due to the fact that the numerous intricate processes and factors can profoundly influence the degree of stimulation, which include amplified spontaneous emission, Rayleigh back-scattering, back-reflection by the fiber ends or splicing points, etc. As a matter of fact, a combination of several of these factors can make the overall SBS process even more cumbersome [7, 8]. In particular, unintended back-reflections can substantially disrupt the conventional framework of SBS, because it can give rise to Brillouin-enhanced four-wave mixing (BEFWM) in addition to SBS. The BEFWM is an optical four-wave mixing (FWM) process mediated by forward-propagating acoustic fields, which does not explicitly rely on the Kerr nonlinearity or the conventional nonlinear refractive index n_2. In addition to the two optical fields of the conventional SBS, it also involves a forward-propagating anti-Stokes field as well as a backward-propagating pump field [9-11]. In fiber systems, an incident optical field can be back-reflected to a considerable degree at points where there is an index mismatch, including fiber ends, splicing points, etc. At extreme power levels, such back-reflections can substantially disrupt the overall SBS [11, 12]. Nevertheless, the effect of BEFWM

on SBS in fiber systems is less apparent or even negligible under low-pump-power conditions, which normally require a relatively long fiber length to give rise to the onset of SBS [11]. This is due to the fact that BEFWM diminishes with the amount of the phase mismatch ΔkL among the interacting forward- and backward-going fields [11], where Δk and L denote the amount of wavenumber mismatch and the fiber length, respectively. In the absence of a sufficient level of birefringence to fulfil the required phase-matching condition, fibers longer than, say, a few meters, are unlikely to keep ΔkL small enough to induce tangible BEFWM. In contrast, under high-pump-power conditions, the onset of SBS can take place within a few meters or even less, irrespective of the existence of built-in birefringence [3, 4, 13]. Given that the demands for fiber systems operating under high-pump-power conditions invariably keep increasing, the impact of BEFWM on SBS warrants a rigorous investigation, in particular, when there is a considerable level of back-reflection [9-11]. Despite this, BEFWM's impact on the SBS threshold in fibers has been overlooked in most cases except for a handful of theoretical and experimental investigations [11, 14, 15]. Here, we theoretically investigate the related matter in a standard single-mode fibers (SMF) via an asymptotic analysis, with which we construct a framework for deducing the power limit and gain conditions for SBS with the influence of BEFWM. This eventually enables us to understand and unveil the detailed consequence of the interplay between SBS and BEFWM in a standard SMF.

The organization of our investigation is thus as follows: First, we investigate whether BEFWM can bring in the Brillouin instability in a standard SMF, using the instability study based on a Laplace transform technique [9]. This instability study is to justify that BEFWM can be approached in terms of a steady-state process in usual circumstances with a standard SMF, in which BEFWM instability hardly takes place except for an extraordinary case of a small $|\Delta kL|$ value. Second, we derive the coupled steady-state equations for Stokes and anti-Stokes fields, and obtain analytical solutions to them. Third, we examine the impact of BEFWM on the SBS threshold and its dependence on fiber length and wave-number mismatch in the presence of Fresnel back-reflection at the fiber's output end as a typical

example. We analyze the asymptotic behavior of the interplay of SBS and BEFWM, deriving the corresponding mathematical formulae to describe it in the infinitesimal and infinite limits of $|\Delta kL|$. Finally, we conclude our theoretical investigation, discussing its potential impact on the design and operation of fiber systems with high-power narrow-linewidth light.

II. BEFWM IN OPTICAL FIBERS AND ITS INSTABILITY

Theoretical studies on the temporal instability induced by BEFWM have been carried out mainly in Brillouin-active liquids for phase-conjugation-mirror applications [9, 10]. To the best of our knowledge, such rigorous studies have yet to be carried out for optical fibers [11, 14, 15]. Thus, in this section we briefly revisit the previous theoretical frameworks and methodologies related to our analysis of the temporal instability of BEFWM, particularly, in optical fibers.

We first describe the theoretical frameworks as the following: We consider a standard silica-based SMF (e.g., SMF-28) as the Brillouin-active medium for investigation. This is supposed to guide forward and backward-pump fields and Stokes and anti-Stokes fields, all of which are tuned to ~ 1550 nm (i.e., the erbium-emission band [16]) as shown in Fig. 1. The Brillouin resonant frequency (Stokes shift) is ~ 11 GHz [17]. Unless stated otherwise, we carry out the investigation under the following assumptions: The forward-pump field has a narrow linewidth well within the Brillouin linewidth of a few tens of MHz; the backward-pump field is generated by Fresnel reflection of the forward-pump field at the rear fiber end terminated in air ($\sim 4\%$) or at a splicing point by the index mismatch as a typical example; there is no back-reflection at the front fiber end for simplicity; the Stokes and anti-Stokes seed fields into the fiber are resonant with the corresponding acoustic fields but substantially weak relative to the forward and backward-pump fields. It is noteworthy that if there is no backward-pump field, the Stokes field will predominantly be generated via conventional SBS by the only forward-pump field [17]. In contrast, if there is a non-negligible backward-pump field accompanied, anti-Stokes scattering of the backward-pump field can occur alongside the Stokes

scattering of the forward-pump field [9-11]. The optical beating among the optical fields further results in the stimulation of acoustic fields, which in turn mediate the FWM among the forward-pump, backward-pump, Stokes, and anti-Stokes fields. All these processes eventually lead to BEFWM, in which longitudinal acoustic waves are assumed to play a dominant role [1]. The key aspect for us to look into in the theoretical investigation that follows is how the interplay between SBS and BEFWM affects the overall SBS process, depending on the effective phase-matching condition for the nonlinear interaction of the four optical fields.

Since the four optical fields involved in the BEFWM are detuned at ~1550 nm by only ~ ±11 GHz in the case of a silica-based standard SMF, we can assume that they have identical mode-field profiles [17]. Their overall optical fields can then be expressed as $E_i^{\pm} = A_i^{\pm}(z,t)\exp\left[i\left(\pm k_i^{\pm} - \omega_i t\right)\right]$, where the subscript i may indicate one of pump, Stokes, or anti-Stokes fields denoted by "p", "s", and "as", respectively. The optical field amplitudes $A_i^{\pm}(z,t)$ take account of the optical field distributions in the transverse plane via a normalization procedure as described in [18]. The positive and negative superscripts denote directions of propagation, parallel and anti-parallel to the forward-pump field, respectively. In total, E_{p}^{+}, E_{p}^{-}, E_{s}^{-}, and E_{as}^{+} are the four optical fields interacting through SBS and BEFWM.

Figures 2(a) and (b) show the energy diagrams and dispersion relations among the optical and acoustic fields, assuming that the acoustic fields are tuned at a single dominant frequency at Ω. In order for BEFWM to be tangible, the four optical fields should interact under near-perfect-phase-matching condition, i.e., $\Delta k = k_{\mathrm{as}}^{+} + k_{\mathrm{p}}^{-} - k_{\mathrm{p}}^{+} - k_{\mathrm{s}}^{-} \sim 0$, if their frequencies are assumed to have already been matched as shown in Fig. 2(a) [9], [17]. A standard SMF with negligible birefringence tends to have a non-zero wavenumber mismatch among the four optical fields owing to the GHz-order Brillouin-resonant-frequency shift, i.e., $\Delta k = 2n\Omega/c$, under the condition that the fiber's dispersion is negligible among them, where c is the speed of light in vacuum and n is the refractive index of the optical fiber. If

the Stokes and anti-Stokes scattering processes occur on the orthogonal principal axes of the optical fiber [15], such as in polarization-maintaining (PM) optical fibers, the wavenumber mismatch is more generally given by $\Delta k = (n_\mathrm{s} + n_\mathrm{f})\Omega/c - 2(n_\mathrm{s} - n_\mathrm{f})\omega_\mathrm{p}/c$, where n_s and n_f denote the refractive indices of the optical fiber along its slow and fast axes, respectively. We can readily calculate the birefringence required for perfect phase-matching by setting $\Delta k = 0$ in the above equation and finding its root, which results in $\sim 8.2 \times 10^{-5}$ for 1550-nm optical fields in a silica-based SMF as shown in Fig. 2(c). (This value is a bit lower than the birefringence of a standard PM SMF [15] although an elliptical-core-based PM fiber may have such a value if its core-cladding index difference is in the order of 0.01 [19].) We can see that the effective interaction length for BEFWM drastically increases across the range where the fiber's birefringence leads to perfect phase-matching. However, it is noteworthy that under normal circumstances of a non-PM standard SMF, the effective interaction length for BEFWM becomes much shorter than a meter, which is the case to which we pay our attention in the investigation that follows.

The nonlinear processes by SBS and BEFWM can be analyzed with the governing equations for the interactions among the four optical fields and the longitudinal acoustic fields induced by Brillouin scattering and FWM, which are derived from Maxwell's equations and the general acoustic wave equation under the slowly-varying envelop approximation as follows [20, 21]:

$$\left(\frac{\partial}{\partial z} + \frac{n}{c}\frac{\partial}{\partial t}\right) A_\mathrm{p}^{+} = i g_\mathrm{o}\left(\rho_\mathrm{s} + \rho_\mathrm{as} e^{i\Delta k z}\right) A_\mathrm{s}^{-}, \tag{1a}$$

$$\left(-\frac{\partial}{\partial z} + \frac{n}{c}\frac{\partial}{\partial t}\right) A_\mathrm{s}^{-} = i g_\mathrm{o}\left(\rho_\mathrm{s}^{*} + \rho_\mathrm{as}^{*} e^{-i\Delta k z}\right) A_\mathrm{p}^{+}, \tag{1b}$$

$$\left(-\frac{\partial}{\partial z} + \frac{n}{c}\frac{\partial}{\partial t}\right) A_\mathrm{p}^{-} = i g_\mathrm{o}\left(\rho_\mathrm{s}^{*} e^{i\Delta k z} + \rho_\mathrm{as}^{*}\right) A_\mathrm{as}^{+}, \tag{1c}$$

$$\left(\frac{\partial}{\partial z} + \frac{n}{c}\frac{\partial}{\partial t}\right) A_\mathrm{as}^{+} = i g_\mathrm{o}\left(\rho_\mathrm{s} e^{-i\Delta k z} + \rho_\mathrm{as}\right) A_\mathrm{p}^{-}, \tag{1d}$$

$$\left(v_\mathrm{a}\frac{\partial}{\partial z} + \frac{\partial}{\partial t}\right) \rho_\mathrm{s} = \left[i\left(\Omega - \Omega_\mathrm{B} - \frac{\Gamma_\mathrm{B}}{2}\right)\right] \rho_\mathrm{s} + i g_\mathrm{a} A_\mathrm{s}^{-*} A_\mathrm{p}^{+}, \tag{1e}$$

$$\left(v_\mathrm{a}\frac{\partial}{\partial z} + \frac{\partial}{\partial t}\right) \rho_\mathrm{as} = \left[i\left(\Omega - \Omega_\mathrm{B} - \frac{\Gamma_\mathrm{B}}{2}\right)\right] \rho_\mathrm{as} + i g_\mathrm{a} A_\mathrm{p}^{-*} A_\mathrm{as}^{+}, \tag{1f}$$

where Ω, Ω_{B} and Γ_{B} denote the acoustic angular frequency, Brillouin resonant angular frequency, and the Brillouin gain bandwidth, respectively; ρ_{s} and ρ_{as} denote the envelopes of the longitudinal acoustic fields inherently driven by Stokes and anti-Stokes scattering processes, respectively; g_{o} and g_{a} denote the Brillouin coupling coefficients for the optical and acoustic fields, respectively. Eqs. (1a) to (1d) describe the spatiotemporal evolutions of the forward-pump, Stokes, backward-pump, and anti-Stokes fields, respectively, whereas Eqs. (1e) and (1f) describe the spatiotemporal evolutions of the acoustic fields, which are driven by electrostriction. The bandwidth Γ_{B} is also equal to the damping constant of the acoustic fields. In general, the spatiotemporal derivative terms in Eqs. (1e) and (1f) can be ignored in the high damping and steady-state condition [21], which is typical for a silica-based SMF. The high acoustic damping means that the acoustic fields are slaved to the optical fields. By contrast, we ignore optical attenuation, because optical loss is negligible within the fiber-length range of our interest. We note that the conventional expression for the Brillouin gain coefficient with respect to optical intensity [22] is given by $\tilde{g}_{\mathrm{B}} = 2g_{\mathrm{o}}g_{\mathrm{a}}/(nc\varepsilon_0\Gamma_{\mathrm{B}})$ in our notation, where ε_0 is the vacuum permittivity and the electrostrictive constant is embedded in g_{a}. The Brillouin gain coefficient typically ranges from 30 to 80 pm/W [23]. The Brillouin gain coefficient can also be represented by g_{B}, which is defined as $g_{\mathrm{B}} = 4g_{\mathrm{o}}g_{\mathrm{a}}/\Gamma_{\mathrm{B}}$ via $g_{\mathrm{B}}\left|A_{\mathrm{p}}^{+}\right|^2 L = \tilde{g}_{\mathrm{B}} I_{\mathrm{p}}^{+} L$, where I_{p}^{+} denotes the intensity of the forward-pump field, for example. In addition, we take the several dimensionless parameters as given in [10]:

$$M_{+} = \tilde{g}_{\mathrm{B}}\left|I_{\mathrm{p}}^{+}\right|^2 L = g_{\mathrm{B}}\left|A_{\mathrm{p}}^{+}\right|^2 L, \tag{2a}$$

$$M_{-} = \tilde{g}_{\mathrm{B}}\left|I_{\mathrm{p}}^{-}\right|^2 L = g_{\mathrm{B}}\left|A_{\mathrm{p}}^{-}\right|^2 L, \tag{2b}$$

$$M = M_{+} + M_{-}, \tag{2c}$$

$$a = \frac{I_{\mathrm{p}}^{-}}{I_{\mathrm{p}}^{+}} = \frac{\left|A_{\mathrm{p}}^{-}\right|^2}{\left|A_{\mathrm{p}}^{+}\right|^2}, \tag{2d}$$

where M_{+} and M_{-} denote the gain factors in neper for the Brillouin Stokes and anti-Stoke scattering, respectively, the a-parameter denotes the ratio of the backward- and forward-pump fields' intensities,

and L denote the length of the fiber under consideration. We note that the impact of BEFWM on SBS is largely determined by M, a, and ΔkL [9, 24].

In addition, we define the nominal power-limit for SBS at which the forward pump power results in a 40-dB gain to the Stokes field without considering the influence by the backward pump [25]. This simply yields $M_+ = 9.21$. Under this condition, pump depletion is still negligible, so that we can use the undepleted pump approximation (UDPA) unless BEFWM instability prevents this. Therefore, we first investigate BEFWM instability in a standard SMF under various conditions for phase mismatch, fiber length, and intensity ratio of the backward and forward-pump fields, to see whether our theoretical approach is justified under the given conditions.

It is known that BEFWM can result in temporal instability in Brillouin-active liquids [9, 10]. When BEFWM-induced temporal instability occurs, the acoustic fields grow immensely, so that the Stokes and anti-Stokes fields are amplified in an extraordinary way until the pump fields are substantially depleted. We note that in the experiments previously reported [9, 10], the total phase mismatch (i.e., ΔkL) was less than 2π and the intensity ratio of the backward and forward-pump fields (i.e., the a-parameter) was larger than 0.1. In contrast, if the Brillouin-active medium is replaced with a standard SMF, the resultant total phase mismatch is unlikely to remain within 2π. For example, 670 rad/m is a typical value for the phase mismatch rate for a standard SMF when operating at $\sim 1550\,\text{-}\,\text{nm}$ wavelength in the absence of birefringence [11]. In addition, we consider that the backward-pump field is generated by ~ 4% Fresnel reflection or splicing-induced back-reflection at the rear end of the fiber under consideration. This means the a-parameter is expected to be significantly smaller than ~ 0.1 under normal circumstances. We stress that these conditions for a standard SMF are radically different from those of the Brillouin-active liquids investigated in [9] and [10], so that it is indeed necessary to determine whether BEFWM instability occurs in normal circumstances with a standard SMF.

The BEFWM instability analysis is carried out based on the Laplace transform method [9]. We first apply both the UDPA and steady-state approximation to Eqs. (1a)–(1d) and then Laplace-transform Eqs. (1b) and (1d) to obtain the equations for the Stokes and anti-Stokes fields in terms of the Laplace conjugate variable "s" [9]. We obtain the closed-form solutions to the equations with poles that can be found numerically in a straightforward manner [26]. The temporal stability or instability of the Stokes and anti-Stokes waves is governed by the location of the poles. In particular, the most significant pole, which has the largest real value among the poles, determines the critical gain factor for the BEFWM instability, i.e., M_{cr} (see [9] for more details). Consequently, if $M > M_{\mathrm{cr}}$, we deduce that BEFWM instability may occur.

The critical gain factor (i.e., M_{cr}) for BEFWM instability in a standard SMF (e.g., SMF-28) is calculated and illustrated in Figs. 3(a) and 3(b) with respect to ΔkL and the a-parameter. The red-dotted lines (M_0) denote the nominal M values simply calculated by the sum of the Stokes and anti-Stokes gain factors, i.e., $M_0 = (1 + a)M_+|_{40\mathrm{dB}}$, where the nominal Stokes gain factor is fixed to 40 dB, i.e., $M_+ = 9.21$. These nominal M values are calculated and illustrated just for comparison. In Fig. 3(a), the growing oscillatory curve ($M_{\mathrm{cr}-4\%}$, black solid line) denotes the case with a backward-pump field, generated by the Fresnel refection of the forward-pump field at the rear fiber end (i.e., $a = 0.04$). With $a = 0.04$, M_{cr} initially decreases from $\Delta kL = 0$ until it reaches the minimum value. It then increases with ΔkL, albeit with rapid oscillations. Except for the interval of $\sim \frac{3\pi}{5} < |\Delta kL| < \sim 2\pi$ (more exactly, $0.6\pi < \Delta kL < 2.2\pi$) [i.e., the range shaded in pink in the inset of Fig. 3(a)], $M_{\mathrm{cr}-4\%}$ is invariably higher than M_0. That is, unless ΔkL reduces to a quantity close to $\sim 2\pi$, M_{cr} becomes much larger than M_0 no matter how large the a-parameter is, as shown in Fig. 3(b). This indicates that except for the interval shaded in pink, the BEFWM instability threshold is invariably and sufficiently higher than the nominal power-limit for SBS, so that the BEFWM instability hardly turns up before the onset of SBS. It is noteworthy that in the absence of birefringence, ΔkL is typically given by $\sim 670\ L$ for a standard

SMF. Thus, this result explains why the BEFWM instability or the related effect is hardly observable under low-pump-power conditions with a relatively long standard SMF. Thus, as far as we avoid the range shaded in pink in Figs. 3(a) and 3(b), we can regard BEFWM as a state-state process, in which transient behaviors in the optical and acoustic fields decay within the steady-state time constant [9, 10] defined by $t_{\mathrm{ss}} \approx 1/[2\mathrm{Re}(s_{\mathrm{ms}})]$, where s_{ms} denotes the complex root for the most significant pole [9, 10].

We have calculated the steady-state time constant with respect to ΔkL for $a = 0.04$, and plot the result in Fig. 3(c): t_{ss} tends to be less than ~ 36.5 ns for any total phase mismatch larger than 4π, and eventually converges to 6.7 ns for even larger values of ΔkL. This time scale is much shorter than the typical temporal duration of a quasi-CW (and true CW) single-frequency pump field that can trigger SBS. In fact, this transient response of BEFWM will rapidly decay down to a steady state within the duration of a quasi-CW optical input. Thus, in a standard SMF, BEFWM can be formulated under the steady-state approximation unless $|\Delta kL|$ reduces to a quantity close to $\sim 2\pi$.

III. THEORY OF SBS-BEFWM COUPLING

In the preceding section, we have shown that effects by the temporal instability and transient response of BEFWM are negligible in most cases with a standard SMF unless $|\Delta kL|$ reduces to a quantity close to $\sim 2\pi$, so that the acoustic field can be considered to be in a steady state. Under this condition, we can convert the coupled partial differential equations, Eqs. (1a) to (1f), into ordinary differential equations [20, 21]. Moreover, we consider a parameter range in which pump depletion is negligible, so that we can obtain their solutions under the UDPA as well. (We note that this theoretical formalism is similar to that of the FWM model previously reported regarding the Brillouin dynamic grating in a PM fiber [14]. Whilst our formalism shares the same governing equation set of Eqs. (1a)–(1f) with the FWM model, it is noteworthy that the focus of our investigation is radically different

from that of the FWM model in that the latter focused on the power evolutions of the backward-pump and anti-Stokes fields with assuming the forward-pump and Stokes fields to be undepleted [14].)

The detailed theoretical formulation of our model is as follows: For steady-state acoustic fields under high damping conditions such as in optical fibers, the derivative terms in Eqs. (1e) and (1f) can be assumed to vanish. Subsequently, the steady-state solutions for ρ_s and ρ_{as} are obtained in a straightforward manner [20, 21]. The total acoustic field is thus represented by the sum of the two acoustic fields' contributions such that $\rho = \rho_s + \rho_{as} e^{i\Delta kz}$, i.e.,

$$\rho = i g_{\mathrm{a}} \frac{A_{\mathrm{S}}^{-*} A_{\mathrm{p}}^{+} + A_{\mathrm{p}}^{-*} A_{\mathrm{as}}^{+} e^{i\Delta kz}}{\frac{\Gamma_{\mathrm{B}}}{2} - i(\Omega - \Omega_{\mathrm{B}})}. \tag{3}$$

In the numerator of Eq. (3), the first and second terms denote the contributions by the Brillouin Stokes and anti-Stokes fields, respectively. If we ignored the second term, this would reduce to the case with simple Stokes scattering without BEFWM. In principle, the second term perturbs the Stokes scattering: Depending on the effective phase mismatch between the two terms, the perturbation can be constructive or destructive to the inherent acoustic driving force by the Stokes scattering. It is noteworthy that the effective phase mismatch is determined not only by Δkz but also by the relative phase differences among the four optical fields under consideration. Thus, the perfect phase-matching condition, i.e., $\Delta k = 0$, does not necessarily result in the constructive interference between the two terms, which will be discussed in more detail in Section IV and Appendix A.

Substituting Eq. (3) into Eqs. (1b) and (1d) under the resonant (i.e., $\Omega = \Omega_{\mathrm{B}}$) and UDPA conditions, we obtain the coupled equations in a contracted form:

$$-\frac{d}{dz} A_{\mathrm{S}}^{-} = \frac{g_{\mathrm{B}}}{2} \left| A_{\mathrm{p}}^{+} \right|^2 A_{\mathrm{S}}^{-} + \frac{g_{\mathrm{B}}}{2} A_{\mathrm{as}}^{+*} A_{\mathrm{p}}^{+} A_{\mathrm{p}}^{-} e^{-i\Delta kz}, \tag{4a}$$

$$-\frac{d}{dz} A_{\mathrm{as}}^{+} = \frac{g_{\mathrm{B}}}{2} \left| A_{\mathrm{p}}^{-} \right|^2 A_{\mathrm{as}}^{+} + \frac{g_{\mathrm{B}}}{2} A_{\mathrm{S}}^{-*} A_{\mathrm{p}}^{+} A_{\mathrm{p}}^{-} e^{-i\Delta kz}. \tag{4b}$$

We note that the first terms of Eqs. (4a) and (4b) represent the contributions by the Brillouin Stokes and anti-Stokes scattering processes, respectively, and that the second terms of them represent the

contributions by the cross-coupling with Stokes and anti-Stokes fields via BEFWM, respectively. To find analytic solutions to the coupled equations, we introduce ansatz functions of self-coupling-compensated Stokes and anti-Stokes fields, such that $\tilde{A}_{\mathrm{s}}^{-}(z) = A_{\mathrm{s}}^{-}(z)\exp\left(\frac{g_{\mathrm{B}}}{2}\left|A_{\mathrm{p}}^{+}\right|^{2} z\right)$ and $\tilde{A}_{\mathrm{as}}^{+}(z) = A_{\mathrm{as}}^{+}(z)\exp\left(\frac{g_{\mathrm{B}}}{2}|A_{\mathrm{p}}^{-}|^{2} z\right)$. Substituting them into Eqs. (4a) and (4b), the SBS-BEFWM-coupled equations become:

$$-\frac{d}{dz}\tilde{A}_{\mathrm{s}}^{-} = \frac{g_{\mathrm{B}}}{2} A_{\mathrm{p}}^{+} A_{\mathrm{p}}^{-} e^{-i\Delta k z} \exp\left[\frac{g_{\mathrm{B}}}{2}\left(\left|A_{\mathrm{p}}^{+}\right|^{2} - \left|A_{\mathrm{p}}^{-}\right|^{2}\right) z\right] \tilde{A}_{\mathrm{as}}^{+*}, \tag{5a}$$

$$-\frac{d}{dz}\tilde{A}_{\mathrm{as}}^{+*} = \frac{g_{\mathrm{B}}}{2} A_{\mathrm{p}}^{+*} A_{\mathrm{p}}^{-*} e^{i\Delta k z} \exp\left[-\frac{g_{\mathrm{B}}}{2}\left(\left|A_{\mathrm{p}}^{+}\right|^{2} - \left|A_{\mathrm{p}}^{-}\right|^{2}\right) z\right] \tilde{A}_{\mathrm{s}}^{-}. \tag{5b}$$

We note that Eqs. (5a) and (5b) form coupled ordinary differential equations with the two variables $\tilde{A}_{\mathrm{s}}^{-}$ and $\tilde{A}_{\mathrm{as}}^{+*}$. The solutions in a closed form can readily be found if boundary conditions are given for the Stokes and anti-Stokes fields, i.e., $A_{\mathrm{s}L}^{-} \equiv A_{\mathrm{s}}^{-}(L)$ and $A_{\mathrm{as0}}^{+*} \equiv A_{\mathrm{as}}^{+*}(0)$, respectively, where L is the length of the fiber under consideration [27]. Then, the Stokes and anti-Stokes fields become:

$$A_{\mathrm{s}}^{-}(z) = \exp\left[-\left(\frac{i\Delta k'}{2} + \frac{g_B}{2}|A_{\mathrm{p}}^{+}|^{2}\right)z\right]\left\{\frac{\cosh(\sigma z) + \frac{i\Delta k'}{2\sigma}\sinh(\sigma z)}{\cosh(\sigma L) + \frac{i\Delta k'}{2\sigma}\sinh(\sigma L)} \exp\left[\left(\frac{i\Delta k'}{2} + \frac{g_B}{2}|A_{\mathrm{p}}^{+}|^{2}\right)L\right] A_{\mathrm{s}L}^{-}\right. \tag{6a}$$

$$\left. + \frac{\frac{g_{\mathrm{B}}}{2} A_{\mathrm{p}}^{+} A_{\mathrm{p}}^{-} \frac{\sinh[\sigma(L-z)]}{\sigma}}{\cosh(\sigma L) + \frac{i\Delta k'}{2\sigma}\sinh(\sigma L)} A_{\mathrm{as0}}^{+*}\right\},$$

$$A_{\mathrm{as}}^{+*}(z) = \exp\left[\left(\frac{i\Delta k'}{2} - \frac{g_B}{2}|A_{\mathrm{p}}^{-}|^{2}\right)z\right]\left\{\frac{-\frac{g_B}{2} A_{\mathrm{p}}^{+*} A_{\mathrm{p}}^{-*} \frac{\sinh(\sigma z)}{\sigma} \exp\left[\left(\frac{i\Delta k'}{2} + \frac{g_B}{2}|A_{\mathrm{p}}^{+}|^{2}\right)L\right]}{\cosh(\sigma L) + \frac{i\Delta k'}{2\sigma}\sinh(\sigma L)} A_{\mathrm{s}L}^{-}\right. \tag{6b}$$

$$\left. + \frac{\cosh[\sigma(L-z)] + \frac{i\Delta k'}{2\sigma}\sinh[\sigma(L-z)]}{\cosh(\sigma L) + \frac{i\Delta k'}{2\sigma}\sinh(\sigma L)} A_{\mathrm{as0}}^{+*}\right\},$$

where $\Delta k'$ and σ are given by

$$\Delta k' = \Delta k + \frac{i}{2} g_{\mathrm{B}}\left(\left|A_{\mathrm{p}}^{+}\right|^{2} - \left|A_{\mathrm{p}}^{-}\right|^{2}\right), \tag{7a}$$

$$\sigma^{2} = \frac{1}{4} g_{\mathrm{B}}^{2}\left|A_{\mathrm{p}}^{+}\right|^{2}\left|A_{\mathrm{p}}^{-}\right|^{2} - \left(\frac{\Delta k'}{2}\right)^{2}. \tag{7b}$$

Finally, the output Stokes and anti-Stokes fields at $z = 0$ and $z = L$, respectively, become:

$$A_S^-(0) = \frac{\exp\left(\frac{i\Delta kL}{2}\right)\exp\left[\frac{g_B}{4}\left(\left|A_p^+\right|^2+\left|A_p^-\right|^2\right)L\right]}{\cosh(\sigma L)+\frac{i\Delta k'}{2\sigma}\sinh(\sigma L)}A_{sL}^- + \frac{\frac{g_B}{2}A_p^+A_p^-\frac{\sinh(\sigma L)}{\sigma}}{\cosh(\sigma L)+\frac{i\Delta k'}{2\sigma}\sinh(\sigma L)}A_{as0}^{+*} \tag{8a}$$

$$\equiv S_{s,B}A_{sL}^- + S_{s,F}A_{as0}^{+*},$$

$$A_{as}^{+*}(L) = \frac{-\frac{g_B}{2}A_p^{+*}A_p^{-*}\frac{\sinh(\sigma L)}{\sigma}\exp(i\Delta kL)}{\cosh(\sigma L)+\frac{i\Delta k'}{2\sigma}\sinh(\sigma L)}A_{sL}^- + \frac{\exp\left(\frac{i\Delta kL}{2}\right)\exp\left[-\frac{g_B}{4}\left(\left|A_p^+\right|^2+\left|A_p^-\right|^2\right)L\right]}{\cosh(\sigma L)+\frac{i\Delta k'}{2\sigma}\sinh(\sigma L)}A_{as0}^{+*} \tag{8b}$$

$$\equiv S_{as,F}A_{sL}^- + S_{as,B}A_{as0}^{+*}.$$

In addition, with these fields, we can also readily obtain the expressions for the output Stokes and anti-Stokes intensities as given by

$$I_s^-(0) = 2nc\varepsilon_0\left[\left|S_{s,B}\right|^2|A_{sL}^-|^2 + \left|S_{s,F}\right|^2|A_{as0}^+|^2 + 2\mathrm{Re}\left(S_{s,B}S_{s,F}^*A_{sL}^-A_{as0}^{+*}\right)\right], \tag{9a}$$

$$I_{as}^+(L) = 2nc\varepsilon_0\left[\left|S_{as,F}\right|^2|A_{sL}^-|^2 + \left|S_{as,B}\right|^2|A_{as0}^+|^2 + 2\mathrm{Re}\left(S_{as,F}S_{as,B}^*A_{sL}^-A_{as0}^{+*}\right)\right]. \tag{9b}$$

IV. NUMERICAL RESUTS AND DISCUSSION

Based on the analytical solutions obtained in the preceding section, we next investigate the impact of the interplay between SBS and BEFWM on the Stokes and anti-Stokes generation via numerical simulations. In these simulations, we choose the simulation parameters and conditions as follows unless stated otherwise: The nominal Brillouin Stokes gain is fixed to 40 dB (i.e., $M_+ = 9.21$); a-parameter is set to 0.04 (i.e., 4% Fresnel reflection,); the input Stokes and anti-Stokes fields arise from white background noise components [28], so that the output Stokes and anti-Stokes intensities are obtained by taking their ensemble average values. It is noteworthy that under the given conditions the corresponding forward- and backward-pump intensities can readily be determined via Eq. (2).

We now consider the Stokes and anti-Stokes intensities, using Eqs. (9a) and (9b). In fact, they depend not only on the total phase mismatch ΔkL, but also on the relative phase relations among A_p^+, A_p^-, A_{sL}^-, and A_{as0}^+. However, we can readily figure out that the contributions by the third terms in Eqs. (9a) and (9b) would eventually vanish if we take the ensemble averages of them, because the input Stokes and anti-Stokes fields are assumed to arise from white background noise components with

random phases [28]. Consequently, we obtain the ensemble-averaged output Stokes and anti-Stokes intensities as given by

$$\overline{I_{\mathrm{s}}^{-}}(0) = \left|S_{\mathrm{s,B}}\right|^2 \overline{I_{\mathrm{s}L}^{-}} + \left|S_{\mathrm{s,F}}\right|^2 \overline{I_{\mathrm{as}0}^{+}}, \tag{10a}$$

$$\overline{I_{\mathrm{as}}^{+}}(L) = \left|S_{\mathrm{as,F}}\right|^2 \overline{I_{\mathrm{s}L}^{-}} + \left|S_{\mathrm{as,B}}\right|^2 \overline{I_{\mathrm{as}0}^{+}}, \tag{10b}$$

where $\overline{I_{\mathrm{s}L}^{-}} = 2nc\varepsilon_0 \overline{|A_{\mathrm{s}L}^{-}|^2}$ and $\overline{I_{\mathrm{as}0}^{+}} = 2nc\varepsilon_0 \overline{|A_{\mathrm{as}0}^{+}|^2}$, both of which can be regarded identical from the statistical perspective since they are assumed to arise from background white noise components [28]. It is noteworthy that the two terms in each of Eqs. (10a) and (10b) respectively denote the contributions by SBS interplayed with BEFWM, and by BEFWM interplayed with SBS, or vice versa.

In Fig. 4, the relative ratios of the output Stokes and anti-Stokes intensities ensemble-averaged at $z = 0$ and $z = L$, are plotted with respect to $|\Delta kL|$, respectively, including both individual and total contributions. Since all the output intensities are normalized by the input Stokes or anti-Stokes intensity, they can be regarded as the corresponding "amplification ratios". In particular, the horizontal black dotted line in Fig. 4(e) denotes the nominal amplification ratio of the output Stokes intensity calculated based on the forward-pump field only, which should remain constant regardless of $|\Delta kL|$, because the nominal Brillouin Stokes gain is fixed to 40 dB. The ranges shaded in pink denote where BEFWM instability may occur and our current analysis is, thus, no longer valid. It is noteworthy that an *x*-axis value at $\frac{|\Delta kL|}{2\pi} = 100$ typically implies a fiber length of ~ 1 m in the case of a standard SMF. We can see an oscillatory behavior of the normalized output Stokes and anti-Stokes intensities with respect to $|\Delta kL|$. Whilst the depth of the oscillation tends to zero for a sufficiently large $|\Delta kL|$, it grows substantially if $|\Delta kL|$ is reduced to a small quantity, particularly, less than $\sim 5 \times 2\pi$. However, when $|\Delta kL| \ll 1$, the normalized output Stokes intensity decreases again. All these features are due to the fact that the acoustic fields generated respectively by the Stokes and anti-Stokes fields interfere depending on their linear and nonlinear phase mismatches via ΔkL, M_+, and a.

First of all, when $|\Delta kL| \ll 1$, the acoustic fields tend to interfere destructively, so that SBS and BEFWM disrupt each other substantially. It is noteworthy that both Stokes and anti-Stokes scatterings are minimized at $\Delta k = 0$. Whilst this may look counterintuitive, it is truly physical in that the amplification of anti-Stokes fields, i.e., the creation of anti-Stokes photons, is the consequence of the annihilation of acoustic phonons created by Stokes scattering from a quantum-mechanical point of view [see Fig. 2(a)], and thus, the destructive interference effect may well be most significant under the perfect phase-matching condition, i.e., $\Delta k = 0$. In fact, its asymptotic behavior in the infinitesimal limit of $|\Delta kL|$ can be formulated by a parabolic curve of $C_0 + D_0(\Delta kL)^2$, where C_0 and D_0 are a simple positive constants determined as $\Delta kL \to 0$ (see Appendix A for more details). If $\Delta kL \neq 0$, we should take account of the additional linear and nonlinear phase evolutions imposed onto the Stokes and anti-Stokes fields, which may or may not lead to a cooperative or quasi-resonant interplay between SBS and BEFWM, depending on the amount of the aggregated phase mismatches among the four optical fields. For example, we can see large growths in both Stokes and anti-Stokes fields within the range where $\sim 2\pi < |\Delta kL| < \sim 5 \times 2\pi$ rad, for example, which is actually the range where the FWM gain and the corresponding nonlinear phase evolution are significant, thereby resulting the phase-pulling effect by the FWM gain under the given conditions, i.e., $M_+ = 9.21$ and $a = 0.04$ (see Appendix C for more details). In fact, the local maxima within the range denote the locations where the interplay between SBS and BEFWM is cooperative or quasi-resonant. Although ρ_s and ρ_{as} are not perfectly phase-matched, they do have a large constructive overlap with each other via the linear and nonlinear phase evolutions between the Stokes and anti-Stokes fields. In contrast, if $|\Delta kL| \gg 1$, the additional nonlinear phase evolutions of the Stokes and anti-Stokes fields apart from the linear phase evolution of ΔkL, almost diminish (particularly when $|\Delta kL| > \sim 5 \times 2\pi$, see Appendix D for more details), so that we can no longer see such a quasi-resonant interplay between SBS and BEFWM. That is, we can only see

simple oscillatory behaviors in the amplification ratios of Stokes and anti-Stokes fields, which become nearly out of phase, because they are inherently anti-resonant processes to each other.

When $|\Delta kL| \gg 1$, we can also figure out that the local maxima of the oscillatory response of the Stokes field are bounded above by an asymptotic curve formulated by $C_\infty + D_\infty(\Delta kL)^{-2}$ (see Appendix B for more details), where C_∞ and D_∞ are simple positive constants determined as $|\Delta kL| \to \infty$. In fact, all the curves additionally drawn in red in Fig. 4 denote the corresponding asymptotes for the upper bounds of the local maxima of the individual oscillatory responses obtained based on the formulae derived in Appendix B. They are indeed in good agreement with the full numerical results. This consequence is due to the fact that the BEFWM is, in nature, a phase-dependent process, so that the evolution of the related field's amplitude is inversely proportional to $|\Delta kL|$ as most processes governed by a phase-matching condition are [29], which in turn result in the inverse square law with respect to $|\Delta kL|$ regarding the corresponding evolution of the related field's intensity: The intensity is obviously proportional to the square of the field's amplitude. The detailed theoretical and mathematical derivations and formulations for this consequence are given in Appendix B.

It is noteworthy that the depths of the oscillatory responses or the upper bounds of the local maxima of the oscillatory responses can be regarded as a measure of the extra gain introduced to the Stokes field by BEFWM if they are normalized by its nominal SBS gain without considering BEFWM. In particular, when $|\Delta kL| \gg 1$, we have already figured out that the upper bounds of the local maxima of the oscillatory responses can be formulated by an asymptotic curve as shown in Fig. 4(e). (We note that the asymptotic curve when $|\Delta kL| \ll 1$ is not of interest in that the extra gain tends to be negative in this case because of the predominant destructive interference effect therein as discussed earlier.) From the perspective of the Stokes field, the total gain factor G_T that the Stokes field undergoes during the SBS-BEFWM process, can intuitively be understood as the sum of the intrinsic gain by SBS and the extra gain by BEFWM, i.e., $\overline{I_\mathrm{S}^-}(0) = \overline{I_{\mathrm{S}L}^-}\exp(G_\mathrm{SBS} + \Delta G_\mathrm{BEFWM})$, from which we can deduce $G_\mathrm{T} = G_\mathrm{SBS} +$

$\Delta G_{\mathrm{BEFWM}}$, where $G_{\mathrm{SBS}} = g_{\mathrm{B}}\left|A_{\mathrm{p}}^{+}\right|^{2}L = M_{+}$. Since the asymptotic curve for $I_{\mathrm{s}}^{-}(0)$ when $|\Delta kL| \gg 1$ has already been found (see Appendix B for more details), it is straightforward to obtain the asymptotic formula for the extra gain factor $\Delta G_{\mathrm{BEFWM}}$ when $|\Delta kL| \gg 1$. In fact, similar to the asymptotic behavior of $\left|S_{\mathrm{s,B}}\right|^{2}$ and $\left|S_{\mathrm{s,F}}\right|^{2}$, the local maxima of $\Delta G_{\mathrm{BEFWM}}$ are also bounded above by $\eta_{\infty}(\Delta kL)^{-2}$, in which there is no offset constant included. It is noteworthy that G_{SBS} is actually the offset constant from the viewpoint of G_{T} (see Appendix B for more details). This implies that the extra gain factor by BEFWM is also inversely proportional to $(\Delta kL)^{2}$. We stress that in normal circumstances, Δk is fixed to a constant value unless the birefringence of the fiber varies along the length, so that the extra-gain effect by BEFWM or the corresponding change to the power-limit for SBS becomes much more apparent as the fiber length becomes shorter as long as the nominal Brillouin Stokes gain through the fiber length can be made as high as 40 dB.

In Fig. 5, we further illustrate the asymptotic behavior of the extra gain factor with respect to $|\Delta kL|$ for several different a-parameter values, including $a = 0.04$, 0.01, 0.001, and 0.0001 under the same conditions for the other parameters. The individual asymptotes theoretically calculated based on $\eta_{\infty}(\Delta kL)^{-2}$, where η_{∞} is the proportional coefficient dependent on M_{+} and a (see Appendix D for more details), are all in excellent agreement with the corresponding traces of the local maxima of the full numerical results when $|\Delta kL| \gg 1$. The extra gain by BEFWM grows with the magnitude of the a-parameter; however, it becomes insignificant if $a < 0.01$ no matter what value of $|\Delta kL|$ becomes.

V. CONCLUSION

By means of theoretical modeling and formulation via statistical and asymptotic approaches, we have investigated the interplay of SBS and BEFWM in a standard SMF in the case when the forward-going pump light is back-reflected at the fiber end in normal circumstances. We have verified that an abnormal SBS modulation can take place via the extra gain caused by BEFWM, which critically

depends on the effective linear and nonlinear phase mismatches via $|\Delta kL|$, M_+, and a. In more detail, we have figured out that when $|\Delta kL| \ll 1$, the acoustic fields ρ_s and ρ_{as} tend to interfere destructively, and thus, SBS and BEFWM are anti-resonant to each other. This tendency eventually results in both Stokes and anti-Stokes scatterings minimized at $\Delta k = 0$. We have also figured out that when $|\Delta kL| \gg 1$, all the asymptotic curves for the amplification ratios and extra gain factor obey the inverse square law with respect to $|\Delta kL|$, irrespective of the level of the back-reflection at the rear fiber. In particular, when $\sim 2\pi < |\Delta kL| < \sim 5 \times 2\pi$, typically for $M_+ = 9.21$ and $a = 0.04$, SBS and BEFWM can be cooperative via the phase-pulling effect by the FWM gain, thereby leading to quasi-resonant growths of both Stokes and anti-Stokes fields. In contrast, when $|\Delta kL| \gg 1$, particularly when $|\Delta kL| > \sim 5 \times 2\pi$, SBS and BEFWM become no longer cooperative, returning to exhibiting anti-resonant oscillatory behaviors without bringing in considerable growths of both Stokes and anti-Stokes fields. This means that for a standard SMF under normal circumstances with the fiber-end's termination, the interplay between SBS and BEFWM is not really tangible unless its length is far below a meter or it has non-negligible birefringence that may make $|\Delta kL|$ less than $\sim 5 \times 2\pi$ rad in the case of $M_+ = 9.21$ and $a = 0.04$, for example. In addition, the extra gain effect by BEFWM fades significantly as the level of the back-reflection reduces to below one percent, i.e., $a < 0.01$.

Inherently, the interplay between SBS and BEFWM is phase-dependent whilst it can still happen with white noise seeding with random phases as discussed in the preceding section. Thus, if the overall phase conditions are readily adjustable with external seeding, the interplay between them can be exploited for all-optical switching functionality as recently demonstrated in [15]. We expect that our theoretical modeling and formulation will be useful for designing and analyzing a variety of fiber systems that incorporate high-power narrow-linewidth light undergoing non-negligible back-reflection under various conditions.

APPENDIX A. ASYMPTOTIC FORMULATION OF AMPLIFICATION RATIOS WHEN $|\Delta kL| \ll 1$

One can see in Fig. 4 that both Stokes and anti-Stokes fields diminish when $|\Delta kL| \ll 1$. This is due to the fact that the acoustic fields ρ_s and ρ_{as} tend to interfere destructively under the perfect phase-matching condition, i.e., $\Delta k = 0$. It is noteworthy that although the nominal FWM gain may be maximized when $\Delta k = 0$, it cannot be warranted that the amplification of anti-Stokes fields is maximized at the same time, because the creation of anti-Stokes photons is the consequence of the annihilation of acoustic phonons created by Stokes scattering from a quantum-mechanical point of view [see Fig. 2(a)]. That is, BEFWM is inherently anti-resonant with SBS. Thus, BEFWM tends to disrupt SBS substantially when the FWM gain is large. Although the interplay between SBS and BEFWM can be cooperative or quasi-resonant in a certain range, e.g., $\sim 2\pi < |\Delta kL| < \sim 5 \times 2\pi$ for $M_+ = 9.21$ and $a = 0.04$, via the linear and nonlinear phase evolutions in the Stokes and anti-Stokes fields together with the FWM gain, the details of which is to be discussed in Appendix C, we, in the following, pay our attention to the asymptotic behavior of the interplay particularly when $|\Delta kL| \ll 1$.

In fact, the linear and nonlinear phase evolutions in the Stokes and anti-Stokes fields are predominantly determined by $\Delta k'L$ and σL, which can be rewritten into

$$\Delta k'L = x + i\delta, \tag{A1a}$$

$$(\sigma L)^2 = \left(\tfrac{1}{2}\right)^2(\delta'^2 - x^2 - i2\delta x), \tag{A1b}$$

where new parameters have been introduced for the sake of notational simplicity such that

$$x \equiv \Delta kL, \tag{A2a}$$

$$\delta = \tfrac{1}{2}g_{\mathrm{B}}\left(\left|A_{\mathrm{p}}^{+}\right|^2 - \left|A_{\mathrm{p}}^{-}\right|^2\right)L, \tag{A2b}$$

$$\delta' = \tfrac{1}{2}g_{\mathrm{B}}\left(\left|A_{\mathrm{p}}^{+}\right|^2 + \left|A_{\mathrm{p}}^{-}\right|^2\right)L. \tag{A2c}$$

It is noteworthy that x is a variable whereas δ and δ' are simple positive constants under the given condition (i.e., $M_+ = 9.21$ and $a = 0.04$).

In fact, the ensemble-averaged output Stokes intensity, which is given by Eq. (10a), is predominantly determined by $\left|S_{\mathrm{s,B}}\right|^2$, because the case considered in this investigation is when $a \ll 1$. We thus pay our attention to the first term of Eq. (10a) in the first place, deriving its asymptotic formula as $|\Delta kL| \to 0$. Once this has been done, the other form for $\left|S_{\mathrm{s,F}}\right|^2$ will also be obtained in a very similar manner without difficulty.

The general expression for $\left|S_{\mathrm{s,B}}\right|^2$ given in Eq. (8a) is now rewritten into the following form:

$$\left|S_{\mathrm{s,B}}\right|^2 = \frac{\exp\left[\frac{1}{2}M_+(1+a)\right]}{\left|\cosh(\sigma L)+\frac{i\Delta k'}{2\sigma}\sinh(\sigma L)\right|^2}, \tag{A3}$$

where the relations given in Eq. (2) have been used for simplifying the numerator. In order to obtain the full asymptotic formula for $\left|S_{\mathrm{s,B}}\right|^2$, we start with representing σL as its own asymptotic formula as $x \to 0$, for which the full expression for σL is now rewritten into

$$\sigma L = +\frac{\delta'}{2}\left[1 - i\left(\frac{2\delta}{\delta'^2}\right)x - \frac{x^2}{\delta'^2}\right]^{\frac{1}{2}}, \tag{A4}$$

where the positive sign has been taken for convention that σ is normally defined to have a positive real part. It is noteworthy that the two values of $\pm\sigma$ obtained from the characteristic equation of Eq. (7b) eventually result in the overall solutions expressed in terms of $\cosh(\sigma z)$ and $\sinh(\sigma z)$ functions regardless of the choice of the sign convention [see Eq. (6)]. Since the full expression already contains a second-order term in terms of x, we can think of representing it by means of a Taylor series expansion up to at least second order. With this mathematical manipulation, we can readily obtain the asymptotic formula for σL when $x \ll 1$ as given by

$$\sigma L \cong \xi_0 - i\xi_1 x - \xi_2 x^2 \quad (|x| \to 0), \tag{A5}$$

where

$$\xi_0 = \frac{\delta'}{2} = \frac{1}{4}M_+(1+a), \tag{A6a}$$

$$\xi_1 = \frac{\delta}{2\delta'} = \frac{1}{2}\left(\frac{1-a}{1+a}\right), \tag{A6b}$$

$$\xi_2 = \frac{1}{4\delta'^3}(\delta'^2 - \delta^2) = \frac{2a}{M_+(1+a)^3}. \quad \text{(A6c)}$$

We then look into all the terms in the denominator of Eq. (A3) within the limit $|\Delta kL| \ll 1$, i.e., $|x| \ll 1$, including the factor $\frac{i\Delta k'}{2\sigma}$ as well as $\cosh(\sigma L)$ and $\sinh(\sigma L)$. First, the full expression for the factor $\frac{i\Delta k'}{2\sigma}$ can be rewritten into

$$\frac{i\Delta k'}{2\sigma} = \frac{i(x+i\delta)}{2\sigma L} = \left(\frac{-\delta}{2}\right)\left(1 - i\frac{x}{\delta}\right)\left(\frac{1}{\sigma L}\right). \quad \text{(A7)}$$

In fact, this relation can also be represented by a Taylor series expansion up to second order via Eq. (A5), so that we obtain the following relation after tedious mathematical manipulations:

$$\frac{i\Delta k'}{2\sigma} \cong -\zeta_0 + i\zeta_1 x - \zeta_2 x^2 \quad (|x| \to 0), \quad \text{(A8)}$$

where

$$\zeta_0 = \frac{\delta}{\delta'} = \frac{1-a}{1+a}, \quad \text{(A9a)}$$

$$\zeta_1 = \frac{1}{\delta'^3}(\delta'^2 - \delta^2) = \frac{8a}{M_+(1+a)^3}, \quad \text{(A9b)}$$

$$\zeta_2 = \frac{3\delta}{2\delta'^5}(\delta'^2 - \delta^2) = \frac{24a(1-a)}{M_+^2(1+a)^5}. \quad \text{(A9c)}$$

As for $\cosh(\sigma L)$ and $\sinh(\sigma L)$, we additionally utilize the following relations since σL is a complex quantity:

$$\cosh(\sigma L) = \cosh[\mathrm{Re}(\sigma L)]\cos[\mathrm{Im}(\sigma L)] + i\sinh[\mathrm{Re}(\sigma L)]\sin[\mathrm{Im}(\sigma L)], \quad \text{(A10a)}$$

$$\sinh(\sigma L) = \sinh[\mathrm{Re}(\sigma L)]\cos[\mathrm{Im}(\sigma L)] + i\cosh[\mathrm{Re}(\sigma L)]\sin[\mathrm{Im}(\sigma L)]. \quad \text{(A10b)}$$

Based on Eqs. (A5) and (A10), we obtain the asymptotic formulae for both $\cosh(\sigma L)$ and $\sinh(\sigma L)$ up to second order in terms of x in a straightforward manner.

After tedious mathematical manipulations with all the individual terms in the denominator of Eq. (A3) and collecting terms up to second order, we eventually obtain

$$\left|\cosh(\sigma L) + \frac{i\Delta k'}{2\sigma}\sinh(\sigma L)\right|^2 \cong \gamma_0^2 - (2\gamma_0\gamma_2 - \gamma_1^2)x^2 \quad (|x| \to 0), \quad \text{(A11)}$$

where

$$\gamma_0 = \cosh(\xi_0) - \zeta_0\sinh(\xi_0), \quad \text{(A12a)}$$

$$\gamma_1 = \zeta_0\xi_1\cosh(\xi_0) - (\xi_1 - \zeta_1)\sinh(\xi_0), \tag{A12b}$$

$$\gamma_2 = \left(\tfrac{1}{2}\xi_1^2 - \zeta_0\xi_2 - \zeta_1\xi_1\right)\cosh(\xi_0) - \left(\tfrac{1}{2}\zeta_0\xi_1^2 - \xi_2 - \zeta_2\right)\sinh(\xi_0). \tag{A12c}$$

Consequently, the asymptotic curve for Eq. (A3) when $|x| \ll 1$ becomes

$$\left|S_{\mathrm{s,B}}\right|^2_{\mathrm{asympt},0} = \exp\left[\tfrac{1}{2}M_+(1+a)\right](C_0 + D_0x^2) \quad (|x| \to 0), \tag{A13}$$

where

$$C_0 = \tfrac{1}{\gamma_0^2}, \tag{A14a}$$

$$D_0 = \tfrac{2\gamma_2}{\gamma_0^3} - \tfrac{\gamma_1^2}{\gamma_0^4}. \tag{A14b}$$

It is noteworthy that excluding a constant, the lowest-order term is second order in terms of x. In other words, $\left|S_{\mathrm{s,B}}\right|^2$ can be represented by $C_0 + D_0x^2$ when $|x| \ll 1$. Since D_0 is inherently a positive quantity under the given condition (i.e., $M_+ = 9.21$ and $a = 0.04$), the asymptotic curve when $|\Delta kL| \ll 1$ becomes a concave-up parabola, which implies its minimum is at the vertex, i.e., at $\Delta kL = 0$, as can be seen from Fig. 4(a). In fact, this consequence is due to the fact that the acoustic fields ρ_s and ρ_{as} interfere destructively when $\Delta k = 0$ or $\Delta k \ll 0$ in that the creation of anti-Stokes photons is the consequence of the annihilation of acoustic phonons created by Stokes scattering from a quantum-mechanical point of view. That is, BEFWM and SBS are inherently anti-resonant processes to each other.

As for $\left|S_{\mathrm{s,F}}\right|^2$, its general expression is given by

$$\left|S_{\mathrm{s,F}}\right|^2 = \frac{\frac{1}{4}aM_+^2\left|\frac{\sinh(\sigma L)}{\sigma L}\right|^2}{\left|\cosh(\sigma L) + \frac{i\Delta k'}{2\sigma}\sinh(\sigma L)\right|^2}. \tag{A15}$$

Since the asymptotic formula for the denominator when $|x| \ll 1$, has already been found, we just need to deal with the numerator in this case. In a similar manner, we obtain the following relation for the numerator part:

$$\left|\tfrac{\sinh(\sigma L)}{\sigma L}\right|^2 \cong U_0 - V_0x^2 \quad (|x| \to 0), \tag{A16}$$

where

$$U_0 = \left(\frac{4}{\delta'^2}\right)\sinh^2\xi_0, \tag{A17a}$$

$$V_0 = \left(\frac{1}{\delta'^4}\right)\left\{\left(\delta^2 + 8\frac{\delta^2}{\delta'^2} - 4\right)\sinh^2\xi_0 + \left(\frac{2}{\delta'}\right)(\delta'^2 - \delta^2)\sinh\xi_0\cosh\xi_0 - \delta^2\cosh^2\xi_0\right\}. \tag{A17b}$$

Consequently, the asymptotic curve for $\left|S_{\mathrm{s,F}}\right|^2$ when $|x| \ll 1$ becomes

$$\left|S_{\mathrm{s,F}}\right|^2_{\mathrm{asympt},0} = \frac{aM_+^2}{4}[C_0U_0 + (D_0U_0 - C_0V_0)x^2] \quad (|x| \to 0). \tag{A18}$$

It is noteworthy that the asymptotic curve for $\left|S_{\mathrm{s,F}}\right|^2$ when $|x| \ll 1$ also becomes a concave-up parabola, because $D_0U_0 - C_0V_0$ is invariably positive under the given condition (i.e., $M_+ = 9.21$ and $a = 0.04$). As a result, the Stokes field still becomes minimized at $\Delta kL = 0$ even with taking the extra term of $\left|S_{\mathrm{s,F}}\right|^2$ into account in the given range, as can be seen in Fig. 4(e).

In similar manners, we can also obtain the other asymptotic curves when $|x| \ll 1$ as given by

$$\left|S_{\mathrm{as,B}}\right|^2_{\mathrm{asympt},0} = \exp\left[-\frac{1}{2}M_+(1+a)\right](C_0 + D_0x^2) \quad (|x| \to 0),$$

$$\left|S_{\mathrm{as,F}}\right|^2_{\mathrm{asympt},0} = \frac{aM_+^2}{4}[C_0U_0 + (D_0U_0 - C_0V_0)x^2] \quad (|x| \to 0).$$

APPENDIX B. ASYMPTOTIC FORMULATION OF AMPLIFICATION RATIOS WHEN $|\Delta kL| \gg 1$

In contrast to the monotonically increasing behaviors of $\left|S_{\mathrm{s,B}}\right|^2$ and $\left|S_{\mathrm{s,F}}\right|^2$ with respect to $|\Delta kL|$ when $|\Delta kL| \ll 1$, they turn into exhibiting oscillatory behaviors when $|\Delta kL| \gg 1$ whilst the depths of the oscillations monotonically decrease as can be seen in Figs. 4(a) and (b). In fact, the local maxima of the oscillatory responses are bounded above by certain asymptotic curves, which can be regarded as a measure of the impact of the interplay between SBS and BEFWM. We here investigate them in more details and discuss how the individual asymptotic curves when $|\Delta kL| \gg 1$ are derived. The derivation procedures for them are similar to those given in Appendix A; however, the key difference is that $|\Delta kL|$ is now much larger than unity, i.e., $|\Delta kL| \gg 1$.

When $|\Delta kL| \gg 1$, i.e., $|x| \gg 1$, the full expression for σL can be rewritten into [see Eq. (A5) for comparison]

$$\sigma L = -i\left(\frac{x}{2}\right)\left[1 + i\left(\frac{2\delta}{x}\right) - \frac{\delta'^2}{x^2}\right]^{\frac{1}{2}}, \tag{B1}$$

where the negative sign has been taken for convention that σ is normally defined to have a positive real part. In a similar manner to what has been done in Appendix A [see Eqs. (A3) and (A4)], the Taylor series expansion of Eq. (B1) in terms of x^{-1} up to second order yields

$$\sigma L \cong \frac{\delta}{2} - \frac{i}{2}\left[x - \frac{1}{2}(\delta'^2 - \delta^2)x^{-1}\right] \quad (|x| \to \infty). \tag{B2}$$

With this relation, we can readily obtain

$$\frac{i\Delta k'}{2\sigma} \cong -\left[1 + \frac{1}{2}(\delta'^2 - \delta^2)x^{-2}\right] \quad (|x| \to \infty). \tag{B3}$$

In addition, $\cosh(\sigma L)$ and $\sinh(\sigma L)$ can also be represented by their real and imaginary parts via Eqs. (A10) and (B2). After tedious mathematical manipulations via Eqs. (B2) and (B3), the full asymptotic expression for the denominator of Eq. (A3) when $|x| \gg 1$ eventually becomes

$$\left|\cosh(\sigma L) + \frac{i\Delta k'}{2\sigma}\sinh(\sigma L)\right|^2 \cong \left|\cosh[\mathrm{Re}(\sigma L)] - \left[1 + \frac{1}{2}(\delta'^2 - \delta^2)x^{-2}\right]\sinh[\mathrm{Re}(\sigma L)]\right|^2 \tag{B4}$$
$$+(\delta'^2 - \delta^2)\left[1 + \frac{1}{4}(\delta'^2 - \delta^2)\right]x^{-2}\sin^2[\mathrm{Im}(\sigma L)] \quad (|x| \to \infty).$$

Since the left-hand side (LHS) of Eq. (B4) is the common expression for all of the amplification ratios given in Eq. (10), this outcome equally applies to all of them. It is noteworthy that the denominator function becomes inherently oscillatory in that the second term of the right-hand side (RHS) of the equality of Eq. (B4) varies periodically with respect to $\mathrm{Im}(\sigma L)$ [see Eq. (B2)] whilst the first term varies monotonically. It is also important to note that the second term is invariably results in a positive quantity since δ'^2 is always greater than δ^2, i.e., $\delta'^2 - \delta^2 = aM_+^2$ [see Eqs. (A2b) and (A2c)]. Thus, from Eq. (B4), we can obtain an inequality within the infinite asymptotic limit as given by

$$\left|\cosh(\sigma L) + \frac{i\Delta k'}{2\sigma}\sinh(\sigma L)\right|^2 \geq \left|\cosh[\mathrm{Re}(\sigma L)] - \left[1 + \frac{1}{2}(\delta'^2 - \delta^2)x^{-2}\right]\sinh[\mathrm{Re}(\sigma L)]\right|^2 \quad (|x| \to \infty), \tag{B5}$$

where the equality holds only when $\sin^2[\mathrm{Im}(\sigma L)] = 0$, i.e., $\mathrm{Im}(\sigma L) = n\pi$ (n is a non-zero integer for $|x| \gg 1$). In other words, when $|x| \gg 1$, the denominator function of Eq. (A3), i.e., Eq. (B4), can have local minima where $\sin^2[\mathrm{Im}(\sigma L)] = 0$ if the term of x^{-2} varies in a sufficiently slow manner within the limit $|x| \gg 1$. In fact, this consequence implies the amplification ratio $\left|S_{\mathrm{s,B}}\right|^2$ can be locally maximized wherever $\sin^2[\mathrm{Im}(\sigma L)] = 0$ while the depth of oscillation monotonically decreases with respect to $|\Delta kL|$, i.e., $|x|$. In result, it is truly important to note that the RHS of the inequality given by Eq. (B5) determines the asymptotic curve by which the trace of the local maxima of $\left|S_{\mathrm{s,B}}\right|^2$ is bounded above.

After tedious mathematical manipulations on the RHS of Eq. (B5) via Eqs. (A10) and (B2), we eventually obtain

$$\left|\cosh[\mathrm{Re}(\sigma L)] - \left[1 + \tfrac{1}{2}(\delta'^2 - \delta^2)x^{-2}\right]\sinh[\mathrm{Re}(\sigma L)]\right|^2 \cong \chi_0^2 - \chi_0\chi_2 x^{-2} \quad (|x| \to \infty), \tag{B6}$$

where

$$\chi_0 = \cosh\left(\tfrac{\delta}{2}\right) - \sinh\left(\tfrac{\delta}{2}\right) = \exp\left(-\tfrac{\delta}{2}\right), \tag{B7a}$$

$$\chi_2 = (\delta'^2 - \delta^2)\sinh\left(\tfrac{\delta}{2}\right). \tag{B7b}$$

Substituting this outcome into Eq. (A3), we finally obtain the asymptotic curve when $|x| \gg 1$, by which the local maxima of $\left|S_{\mathrm{s,B}}\right|^2$, are bounded above such that

$$\left|S_{\mathrm{s,B}}\right|^2_{\mathrm{asympt},\infty} = \exp\left[\tfrac{1}{2}M_+(1+a)\right](C_\infty + D_\infty x^{-2}) \quad (|x| \to \infty), \tag{B8}$$

where

$$C_\infty = \tfrac{1}{\chi_0^2} = \exp\left[\tfrac{1}{2}M_+(1-a)\right], \tag{B9a}$$

$$D_\infty = \tfrac{\chi_2}{\chi_0^2} = aM_+^2\exp\left[\tfrac{3}{4}M_+(1-a)\right]\sinh\left[\tfrac{1}{4}M_+(1-a)\right]. \tag{B9b}$$

It is noteworthy that excluding a constant, the lowest-order term is second order in terms of x^{-1}. In other words, the local maxima of $\left|S_{\mathrm{s,B}}\right|^2$ are bounded above by $C_\infty + D_\infty x^{-2}$.

As for the asymptotic curve by which the local maxima of $\left|S_{\mathrm{s,F}}\right|^2$ are bounded above when $|x| \gg 1$, we just need to figure out when the numerator part of Eq. (A15) is maximized in addition. When $|x| \gg 1$, the asymptotic formula of the numerator part except for the constant factor can be rewritten into

$$\left|\frac{\sinh(\sigma L)}{\sigma L}\right|^2 \cong \frac{\sinh^2[\mathrm{Re}(\sigma L)]+\sin^2[\mathrm{Im}(\sigma L)]}{[\mathrm{Re}(\sigma L)]^2+[\mathrm{Im}(\sigma L)]^2} \quad (|x| \to \infty). \tag{B10}$$

Since this function is locally maximized when $\sin^2[\mathrm{Im}(\sigma L)] = 1$, i.e., $\mathrm{Im}(\sigma L) = \frac{1}{2}(2n+1)\pi$ (n is an integer), we can deduce the following inequality within the infinite asymptotic limit after representing all the terms with Taylor series expansions up to second order in terms of x^{-1}:

$$\left|\frac{\sinh(\sigma L)}{\sigma L}\right|^2 \leq 4\cosh^2\left[\tfrac{1}{4}M_+(1-a)\right]x^{-2} \quad (|x| \to \infty). \tag{B11}$$

Substituting Eqs. (B5) and (B11) into Eq. (A15) via Eqs. (B6) and (B8) and collecting all the terms up to second order in terms of x^{-1}, we eventually obtain the asymptotic curve when $|x| \gg 1$ as given by

$$\left|S_{\mathrm{s,F}}\right|^2_{\mathrm{asympt},\infty} = aM_+^2\cosh^2\left[\tfrac{1}{4}M_+(1-a)\right]C_\infty x^{-2} \quad (|x| \to \infty), \tag{B12}$$

It is noteworthy that whilst the minima of the LHS of Eq. (B5) and the maxima of the LHS of Eq. (B11) do not take place exactly at the same locations, the asymptotic curve of Eq. (B12) is still valid in the limit $|x| \gg 1$.

In similar manners, we can also obtain the other asymptotic curves when $|x| \gg 1$ as given by

$$\left|S_{\mathrm{as,F}}\right|^2_{\mathrm{asympt},\infty} = aM_+^2\cosh^2\left[\tfrac{1}{4}M_+(1-a)\right]C_\infty x^{-2},$$

$$\left|S_{\mathrm{as,B}}\right|^2_{\mathrm{asympt},\infty} = \exp\left[-\tfrac{1}{2}M_+(1+a)\right](C_\infty + D_\infty x^{-2}).$$

APPENDIX C. PHASE-PULLING EFFECT BY THE FWM GAIN UNDER QUASI-RESONANT CONDITION

Whilst under the perfect phase-matching condition, the interplay between SBS and BEFWM is exactly anti-resonant, we can see some quasi-resonant behavior particular when $\sim 2\pi$ rad $< |\Delta kL| < \sim 5 \times 2\pi$ rad as shown in Fig. 4. This consequence is due to the fact the common denominator function expressed by $\left|\cosh(\sigma L) + \frac{i\Delta k'}{2\sigma}\sinh(\sigma L)\right|^2$ is sustainably reduced to a very small quantity like what normally happens under resonant condition [21]. In fact, when $|\Delta kL| \gg 1$, i.e., $|x| \gg 1$, the common denominator function is represented by Eq. (B4), which is further reduced to Eq. (B6) particularly when $\mathrm{Im}(\sigma L) = n\pi$ (n is a non-zero integer). In Appendix B, the consequence by the term of x^{-2} in Eq. (B4) has been excluded under the assumption that x is sufficiently larger than unity, i.e., $|x| \gg 1$. This actually leads to the characteristic equation for determining the n-th local maximum as given by

$$x_n - \tfrac{1}{2}(\delta'^2 - \delta^2)x_n^{-1} = 2n\pi \quad (n \text{ is a non-zero integer}). \tag{C1}$$

Under the condition when $|x| \gg 1$, we can readily obtain the solution to Eq. (C1) as given by

$$x_n = n\pi\left\{1 + \left[1 + \tfrac{1}{2}a\left(\tfrac{M_+}{n\pi}\right)^2\right]^{\frac{1}{2}}\right\} \quad (n \text{ is a non-zero integer}). \tag{C2}$$

This solution eventually converges to $x_n \cong 2n\pi$ for a sufficiently large x, i.e., $|x| \gg 1$. For example, we can readily see in Fig. 4(e) that the fifth local maximum takes place nearly at $x \cong 5 \times 2\pi$, which is typically in the case for $M_+ = 9.21$ and $a = 0.04$.

In contrast, if we suppose that x is within the quasi-resonant regime, i.e., when $\sim 2\pi < x < \sim 5 \times 2\pi$, the situation becomes slightly different in that x is rather in the lower part of the range defined by $|x| \gg 1$. Thus, to be more specific, we should take account of both the x^{-2} term and the additive sinusoidal term at the same time in dealing with Eq. (B4). Although we can numerically find where the most significant local maximum takes place in Fig. 4(e), the result can also be obtained by an asymptotic approach that follows. In fact, the additive sinusoidal term can be represented by its zeroth-

order Taylor series expansion via $x_m = 2m\pi + x'$ where m is the largest integer number making x' as small as possible while making x_m be the location for the most significant local maximum, because there is already a second-order infinitesimal factor of x^{-2} in front of it. Substituting the zeroth-order correction term into Eq. (B4) and finding the root which makes the full equation zero, we obtain

$$x_m = \frac{(\chi_0\chi_2 - \chi_S)^{\frac{1}{2}}}{\chi_0}, \tag{C3}$$

where

$$\chi_S = (\delta'^2 - \delta^2)\left[1 + \tfrac{1}{4}(\delta'^2 - \delta^2)\right]\sin^2\left(\tfrac{\delta'^2 - \delta^2}{8n\pi}\right). \tag{C4}$$

In fact, this relation determines where the most significant quasi-resonance takes place. With $m = 2$, the result of Eq. (C3) yields $1.88 \times 2\pi$, whilst the result calculated by Eq. (C2) yields $2.02 \times 2\pi$. For comparison, the full numerical result for the most significant quasi-resonance is given by $1.89 \times 2\pi$. This means the prediction by the asymptotic approach is really of high accuracy.

Moreover, the discrepancy between the results predicted by Eqs. (C2) and (C3) actually unveil that there is a phase-pulling effect in the interplay between SBS and BEFWM, which is caused by the significant FWM gain within its gain bandwidth like the frequency-pulling effect which normally occurs in the resonance of a laser cavity oscillation [30]. Similar to the laser gain, the FWM gain induces the phase-pulling effect towards its peak. The phase-pulling effect gradually diminishes with a factor of x^{-2} beyond the range where the FWM gain is significant. Consequently, for sufficiently large values of x beyond the quasi-resonant regime, the locations of the local maxima can simply be determined by the formula given by Eq. (C2) as can be seen in Fig. 4(e). In this case, there is no significant phase-pulling effect in the interplay between SBS and BEFWM, so that we can eventually see that the local maxima of anti-Stokes fields simply take place where there are the local minima of Stokes fields. SBS and BEFWM are inherently anti-resonant processes to each other as pointed out in Section IV or Appendix A. In fact, the upper limit of the quasi-resonant regime of $\sim 5 \times 2\pi$ has been determined in this respect.

APPENDIX D. ASYMPTOTIC EXTRA-GAIN FACTOR FOR STOKES INTENSITY WHEN $|\Delta kL| \gg 1$

The extra-gain factor for the Stokes intensity can be defined from $\overline{I_s}(0) = \overline{I_{sL}}\exp(G_{\mathrm{SBS}} + \Delta G_{\mathrm{BEFWM}})$ such that

$$\Delta G_{\mathrm{BEFWM}} = \ln\left(\frac{\overline{I_s}(0)}{\overline{I_{sL}}\exp(G_{\mathrm{SBS}})}\right), \tag{D1}$$

where G_{SBS} is the nominal gain factor by SBS without taking account of BEFWM, which is equal to M_+ in our notation. Since $\overline{I_s}(0)$ is given by Eq. (10a) and the asymptotic formulae for the local maxima of $\left|S_{\mathrm{s,B}}\right|^2$ and $\left|S_{\mathrm{s,F}}\right|^2$ when $|x| \gg 1$ are as given by Eqs. (B8) and (B12), we can readily obtain

$$\left.\frac{\overline{I_s}(0)}{\overline{I_{sL}}}\right|_{\mathrm{asympt},\infty} = \exp\left[\tfrac{1}{2}M_+(1+a)\right] C_\infty(1+\eta_\infty x^{-2}) \quad (|x| \to \infty), \tag{D2}$$

where

$$\eta_\infty = \frac{D_\infty}{C_\infty} + aM_+^2 \cosh^2\left[\tfrac{1}{4}M_+(1-a)\right] \exp\left[-\tfrac{1}{2}M_+(1+a)\right] \frac{\overline{I_{\mathrm{as0}}}}{\overline{I_{sL}}}. \tag{D3}$$

It is noteworthy that since both initial Stokes and anti-Stokes fields are assumed to arise from white background noise components, $\frac{\overline{I_{\mathrm{as0}}}}{\overline{I_{sL}}}$ can be set to unity from the statistical point of view. Substituting Eq. (D2) into Eq. (D1), we eventually obtain the asymptotic extra-gain factor for the Stokes intensity when $|x| \gg 1$ as given by

$$\Delta G_{\mathrm{BEFWM}}|_{\mathrm{asympt},\infty} = \ln(1+\eta_\infty x^{-2}) \cong \eta_\infty x^{-2} \quad (|x| \to \infty), \tag{D4}$$

where a Taylor series expansion of the natural logarithmic function up to second order in terms of x^{-1} has been used. It is noteworthy that asymptotic extra-gain factor for the Stokes intensity when $|x| \gg 1$ is invariably formulated by a function of $\eta_\infty x^{-2}$. Moreover, the asymptotic formulations based on the Taylor series expansions up to second order in terms of $(\Delta kL)^{-1}$ are in excellent agreement with the full numerical results as can be verified in Fig. 5.

REFERENCES

[1] K. Park and Y. Jeong, Opt. Express **22**, 7932–7946 (2014).

[2] A. V. Harish and J. Nilsson, Opt. Express **23**, 6988–6999 (2015).

[3] Y. Jeong, *et al.*, IEEE J. Sel. Top. Quantum Electron. **13**, 546–551 (2007).

[4] L. Huang, *et al.*, Opt. Lett. **42**, 1–4 (2017).

[5] A. V. Harish and J. Nilsson, Opt. Eng. **58**, 102703 (2019).

[6] G. D. Goodno and J. E. Rothenberg, Opt. Express **27**, 13129–13141 (2019).

[7] M. Ferrario, *et al.*, Opt. Express **17**, 18110–18115 (2009).

[8] M. Karow, J. Neumann, D. Kracht and P. Weßels, Opt. Express **20**, 10572–10582 (2012).

[9] A. Scott and K. Ridley, IEEE J. Quantum Electron. **25**, 438–459 (1989).

[10] D. E. Watkins, A. M. Scott and K. D. Ridley, IEEE J. Quantum Electron. **26**, 2130–2137 (1990).

[11] K. Park, A. V. Harish, J. Nilsson, and Y. Jeong, SeM4E.4 in *Optical Sensors* (New Orleans, USA, 2017).

[12] M. S. Bowers and N. M. Luzod, Opt. Eng. **58**, 102702 (2019).

[13] C. Zeringue, *et al.*, Opt. Express **20**, 21196-21213 (2012)

[14] D.-P. Zhou, Y. Dong, L. Chen, and X. Bao, Opt. Express **19**, 20785–20798 (2011).

[15] Y. Okawa and K. Hotate, Opt. Lett. **45**, 3406–3409 (2020).

[16] Y. S. Jeong and C. H. Kim, Curr. Opt. Photonics **4**, 472–476 (2020).

[17] G. P. Agrawal, *Nonlinear fiber optics*, 5th ed. (Academic Press, Oxford, 2013).

[18] C. M. de Sterke, K. R. Jackson, and B. D. Robert, J. Opt. Soc. Am. B. **8**, 403–412 (1991).

[19] I.-K. Hwang, Y.-H. Lee, K. Oh, and D. N. Payne, Opt. Express **12**, 1916–1923 (2004).

[20] A. Kobyakov, M. Sauer, and D. Chowdhury, Adv. Opt. Photonics **2**, 1–59 (2010).

[21] R. W. Boyd, *Nonlinear optics*, 3th ed. (Elsevier, Oxford, 2008).

[22] Z. Zhu, *et al*., J. Opt. Soc. Am. B. **22**, 2378–2384 (2005).

[23] M. Nikles, L. Thevenaz, and P. A. Robert, J. Light. Technol. **15**, 1842–1851 (1997).

[24] M. Damzen, V. Vlad, A. Mocofanescu, and V. Babin, *Stimulated Brillouin scattering: fundamentals and applications* (CRC press, FL, USA, 2003).

[25] A. V. Harish, K. Park, Y. Jeong, and J. Nilsson, in *2016 IEEE Photonics Conference* (Waikoloa, HI, USA, 2016).

[26] T. H. Cormen, C. E. Leiserson, R. L. Rivest, and C. Stein, *Introduction to algorithms*, 3rd ed. (MIT press, Cambridge, 2009).

[27] B. Lee and Y. Jeong, Chap. 7 in *Fiber Optic Sensors* (F. T. S. Yu and S. Yin Ed., Marcel Dekker, New York, 2002).

[28] R. W. Boyd, K. Rzaewski, and P. Narum, Phys. Rev. A **42**, 5514 (1990).

[29] A. Yariv and P. Yeh, *Optical Waves in Crystals* (John Wiley, New York, 1984).

[30] A. Yariv, *Optical Electronics*, 4th ed. (Oxford University press, London, 1995).

Figure Captions.

Fig. 1. Schematic of SBS and BEFWM by the forward- and backward-pump fields in an optical fiber.

Fig. 2. BEFWM in a standard SMF: (a) Energy diagram for BEFWM, where $|e_{\mathrm{as}}\rangle$, $|e_{\mathrm{p}}\rangle$, $|i\rangle$, and $|g\rangle$ denote the virtual states for the anti-Stokes and forward-pump fields, the vibration state for the acoustic field, and the ground state, respectively. (b) Frequency and phase-matching diagram for BEFWM based on the optical and acoustic fields' dispersion relations. (c) Phase mismatch Δk and effective interaction length of BEFWM L_{int} with respect to birefringence B. The ranges shaded in pink (i.e., $\sim \frac{3\pi}{5} < |\Delta kL| < \sim 2\pi$) denote where BEFWM instability may occur and our current analysis is, thus, no longer valid.

Fig. 3. Critical gain factor of BEFWM-induced temporal instability in various conditions: (a) Critical gain factor with respect to ΔkL for $a = 0.04$. The red-dotted line denotes the nominal M value, i.e., M_0, for comparison. The inset displays the magnified view of the power limit for small values of ΔkL. (b) Critical gain factor with respect to a for $\frac{\Delta kL}{2\pi} = 1$, 10, and 100. The red-dotted line denotes the nominal M value, i.e., M_0, for comparison. (c) Steady state time constant of BEFWM's transient response for $a = 0.04$.

Fig. 4. Asymptotic behaviors of the amplification ratios of the ensemble-averaged output Stokes and anti-Stokes intensities: (a) $|S_{\mathrm{s,B}}|^2$, (b) $|S_{\mathrm{as,F}}|^2$, (c) $|S_{\mathrm{s,F}}|^2$, (d) $|S_{\mathrm{as,B}}|^2$, (e) $|S_{\mathrm{s,B}}|^2 + |S_{\mathrm{s,F}}|^2$, and (f) $|S_{\mathrm{as,F}}|^2 + |S_{\mathrm{as,B}}|^2$. The red-solid lines denote the corresponding asymptotic curves based on the formulae obtained from Appendices A and B. The ranges shaded in pink (i.e., $\sim \frac{3\pi}{5} < |\Delta kL| < \sim 2\pi$)

denote where BEFWM instability may occur and our current analysis is, thus, no longer valid. The insets display the magnified views of the corresponding ranges.

Fig. 5. The extra-gain factors to the local maxima of the Stokes intensity (scatter points) and the corresponding asymptotic extra-gain factors (solid lines) with respect to $\frac{\Delta kL}{2\pi}$ for $a = 0.04$, 0.01, 0.001, and 0.0001. The individual asymptotic curves are formulated by $\eta_\infty(\Delta kL)^{-2}$, where η_∞ is determined with the corresponding a-paramter (see Appendix D for more details).

Fig. 1

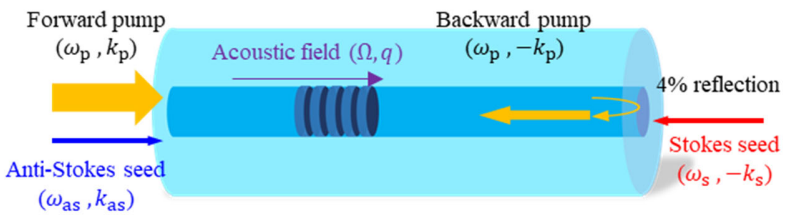
Forward pump
(ω_p, k_p)
Acoustic field (Ω, q)
Backward pump
$(\omega_p, -k_p)$
4% reflection
Stokes seed
$(\omega_s, -k_s)$
Anti-Stokes seed
(ω_{as}, k_{as})

Fig. 2

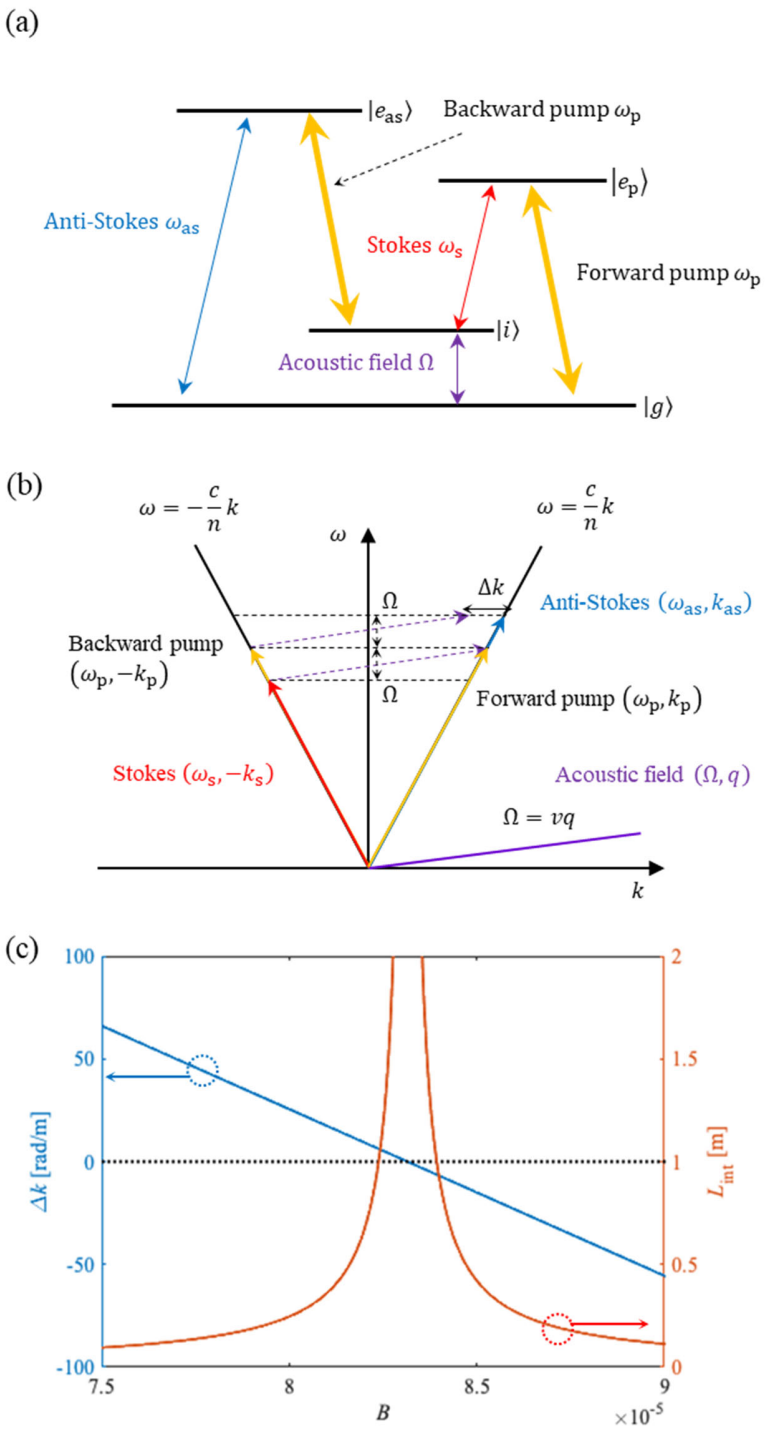
(a)
$|e_{as}\rangle$
Backward pump ω_p
$|e_p\rangle$
Anti-Stokes ω_{as}
Stokes ω_s
Forward pump ω_p
$|i\rangle$
Acoustic field Ω
$|g\rangle$
(b)
$\omega = -\frac{c}{n}k$
$\omega = \frac{c}{n}k$
ω
Ω
Δk
Anti-Stokes (ω_{as}, k_{as})
Backward pump $(\omega_p, -k_p)$
Ω
Forward pump (ω_p, k_p)
Stokes $(\omega_s, -k_s)$
Acoustic field (Ω, q)
$\Omega = vq$
k
(c)
100
50
0
-50
-100
Δk [rad/m]
2
1.5
1
0.5
0
L_{int} [m]
7.5
8
8.5
9
B
$\times 10^{-5}$

Fig. 3

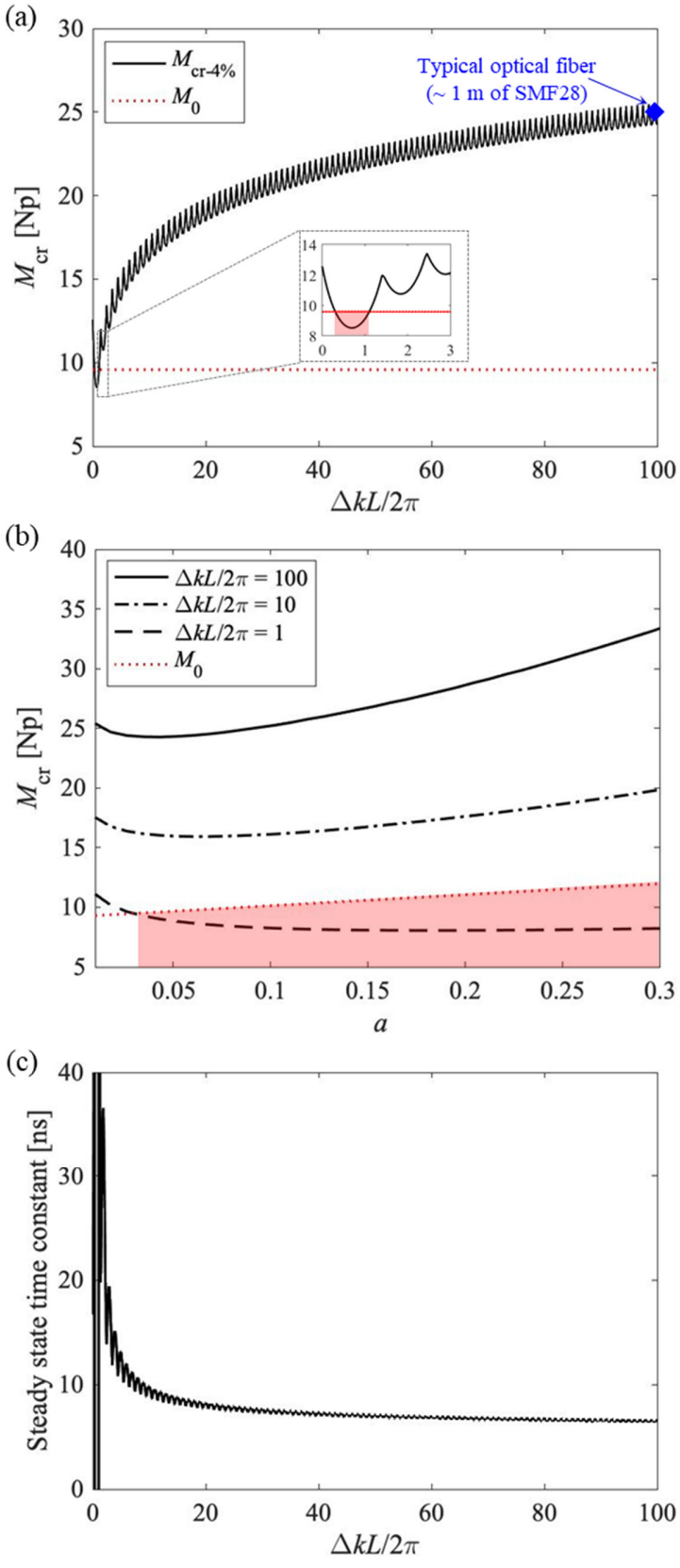
(a)
$M_{cr\text{-}4\%}$
M_0
Typical optical fiber
(~ 1 m of SMF28)
M_{cr} [Np]
$\Delta kL/2\pi$
(b)
$\Delta kL/2\pi = 100$
$\Delta kL/2\pi = 10$
$\Delta kL/2\pi = 1$
M_0
M_{cr} [Np]
a
(c)
Steady state time constant [ns]
$\Delta kL/2\pi$

Fig. 4

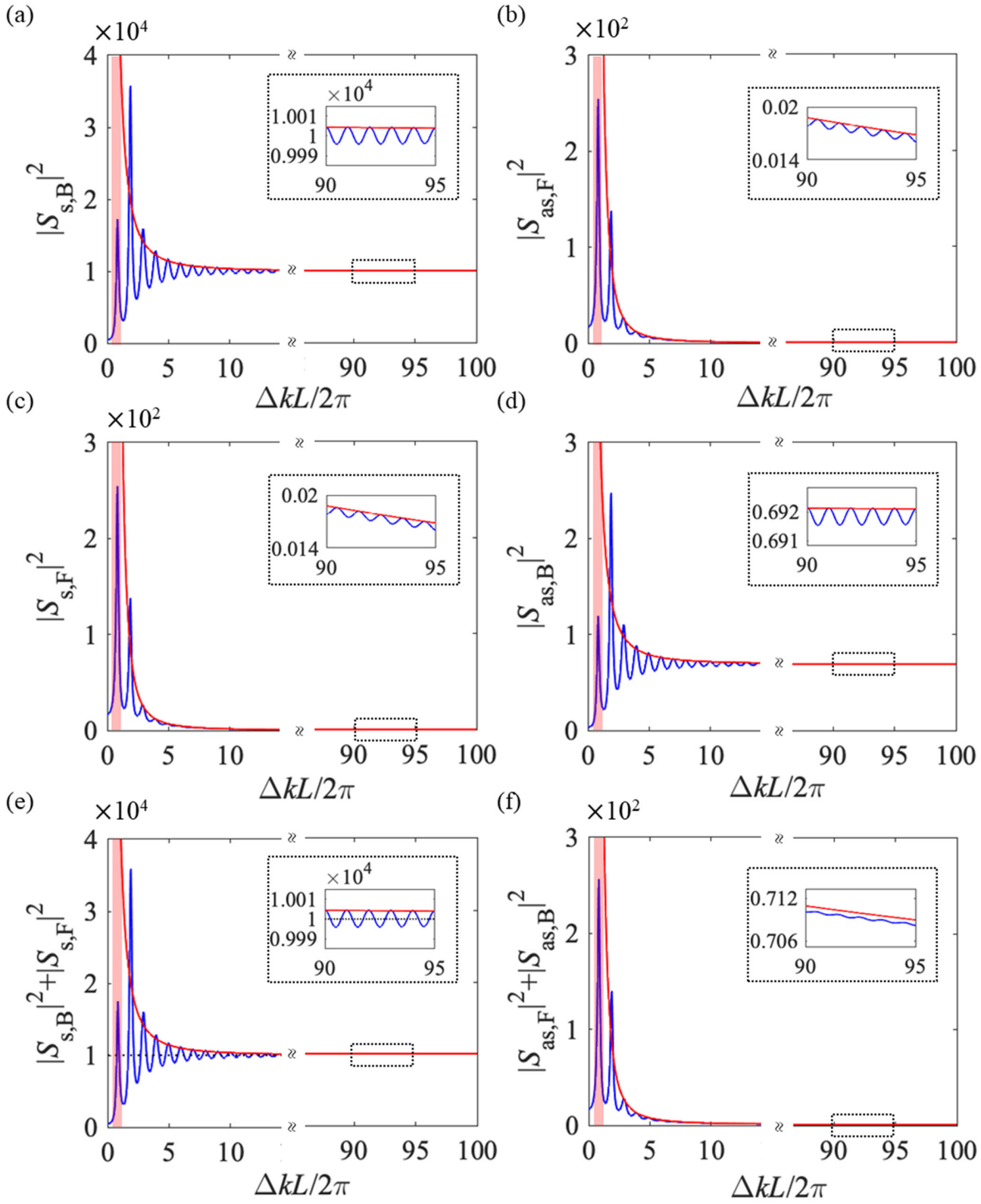
(a)
(b)
(c)
(d)
(e)
(f)
$\Delta kL/2\pi$
$|S_{s,B}|^2$
$|S_{as,F}|^2$
$|S_{s,F}|^2$
$|S_{as,B}|^2$
$|S_{s,B}|^2+|S_{s,F}|^2$
$|S_{as,F}|^2+|S_{as,B}|^2$
×10⁴
×10²
1.001
1
0.999
0.02
0.014
0.692
0.691
0.712
0.706
90
95
100

Fig. 5

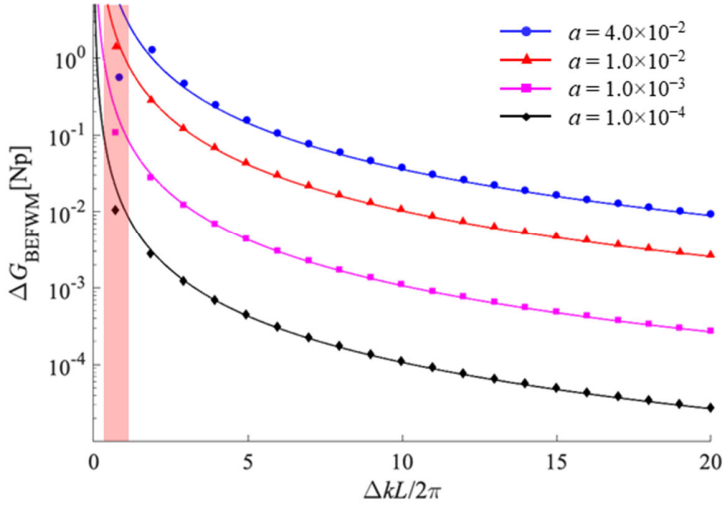
$a = 4.0\times10^{-2}$
$a = 1.0\times10^{-2}$
$a = 1.0\times10^{-3}$
$a = 1.0\times10^{-4}$
10^{0}
10^{-1}
10^{-2}
10^{-3}
10^{-4}
$\Delta G_{\mathrm{BEFWM}}$[Np]
0
5
10
15
20
$\Delta kL/2\pi$